LANGMUIR

pubs.acs.org/Langmuir Article

Structure and Dynamics of Electric-Field-Driven Convective Flows at the Interface between Liquid Electrolytes and Ion-Selective Membranes

Alexander Warren,[§] Arpita Sharma,[§] Duhan Zhang, Gaojin Li, and Lynden A. Archer*

Cite This: *Langmuir* 2021, 37, 5895–5901 Read Online

ACCESS | Metrics & More | Article Recommendations | Supporting Information

ABSTRACT: At voltages above a certain critical value, $V_c \approx 20$ kT/e, a space charge layer forms near ion-selective interfaces in liquid electrolytes. Interactions between the space charge and an imposed electric field drives a hydrodynamic instability known as electroconvection. Through particle tracking velocimetry we experimentally study the structure and dynamics of the resultant electroconvective flow. Consistent with previous numerical simulations, we report that, following imposition of a sufficiently large voltage, electroconvection develops gradually as pairs of counter-rotating vortices, which nucleate at the interface between an ion-selective substrate and a liquid electrolyte. Depending on the imposed voltage and cell geometry, the vorticies grow to length scales of hundreds of micrometers. Electroconvective flows are also reported to be structured and multiscale, with the size ratio of the largest to the smallest observable vortices inversely proportional to the Debye screening length.

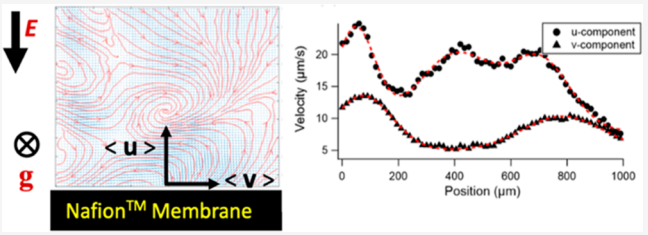

INTRODUCTION

Electric field-driven transport of ions in an electrolyte bounded by at least one ion-selective planar interface is conventionally thought to be limited by electroneutrality. In particular, when the ion depletion rate at the interface exceeds the rate of resupply from the bulk electrolyte, a diffusion limiting current, $i_L = \frac{4zcFD}{L}$ is reached, wherein any additional flux of ions across the interface is resisted by a large electric field that preserves electroneutrality.[1] Here c, z, and D are the salt concentration, mobile ion valency, and diffusivity, respectively; L is the inter electrode spacing, and F is Faraday's constant. A significant body of early work showed that currents appreciably higher than i_L can be sustained by driving the operating potential in the cell to values substantially above the thermal voltage, $V_T = \frac{kT}{e} \sim 26$ mV at 300 K.[2−4] Complications associated with faradaic currents produced by redox chemistry of water initially prevented a full understanding of the origins of such *overlimiting* conductance.[3,5,6] It is currently understood that the source of the behavior is the hydrodynamic instability termed *electroconvection*, an electro-osmotic flow driven by forces originating from coupling of the electric field and concentration polarization in electrolytes at ion-selective interfaces.[7−10] Since its first analysis by Rubinstein et al.,[9,11] electroconvection has been reported in a wide variety of systems like metal electroplating,[12,13] high-energy density batteries,[14] electrodialysis,[15] and water desalination.[16] Furthermore, it is now known that while electroconvection may be advantageous in certain cases like electrodialysis, where it can provide an additional mode of mass transfer, it is undesirable in metal batteries galvanostatically charged at $i > i_L$, where a coupling between electroconvection and morphological instabilities can exacerbate rough deposition in non-planar, dendritic structures. This can lead to battery short circuits, limiting battery life and, in volatile liquid electrolytes, posing serious safety concerns. Therefore, understanding electroconvection and developing techniques to manipulate the flow (e.g., to suppress it,[17,18] or to enhance, based on the system[19]) are important from both fundamental research and application standpoints.

The origin of electroconvection is attributed to the formation of an extended space charge layer (ESCL), many times the length of the equilibrium double layer, which couples to the local electric field inside an electrochemical cell to provide a body force, to drive fluid motion. The thickness of the ESCL (ϵ) depends on the relative voltage ($\hat{V} \equiv V/V_T$) and Debye screening length ($\hat{\delta} = \delta/L$) and varies as $\epsilon \approx L(V\hat{\delta})^{2/3}$.[11] Direct numerical studies by Mani and co-workers have shown that at voltages less than around 20 V_T , electroconvection manifests as paired vortex structures that initiate at the ion-selective interface and grow into the interelectrode space to

Received: February 7, 2021
Revised: April 26, 2021
Published: May 7, 2021

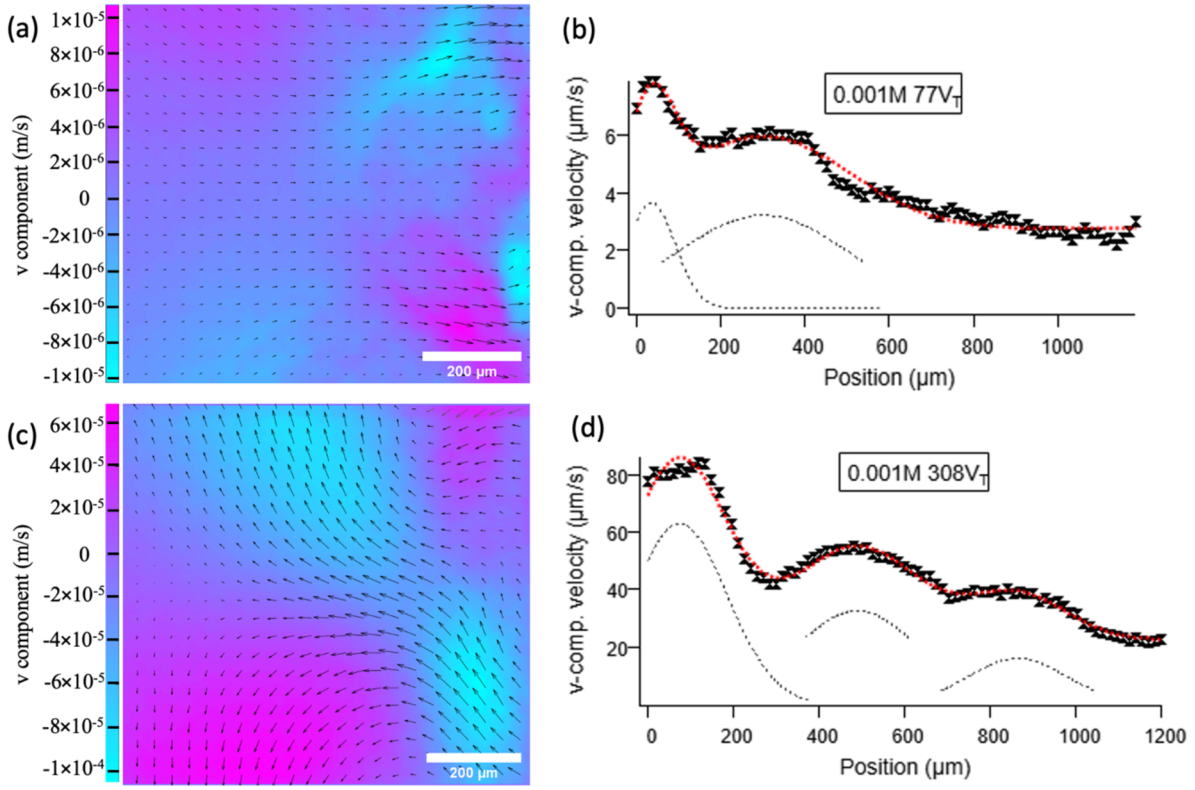

Figure 1. Effects of voltage on the electroconvective structures in 0.001 M $CuSO_{4\ (aq)}$ electrolytes for a 77 V_T (a, b) and 308 V_T (c, d) potential difference across the cell. (a, c) Vector maps with colors depicting the strength and sign of the velocity component parallel to the membrane (v-component). The Nafion membrane ($x = 0$) is on the right side of these maps. (b, d) Profiles of the root-mean-squared velocity component (v_{rms}) as a function of position. It can be seen from the profiles that the first peak velocity magnitude changes from approximately 8 to 80 μm/s as voltage increases from 77 V_T to 308 V_T.

enhance mixing within the electrolyte.[20,21] At higher voltages, the electroconvective flows become multiscale and chaotic.[22,23] Theoretical studies have also investigated coupling of electroconvection with imposed shear flows and gravity. Kwak et al. studied electroconvection in the presence of an externally imposed shear flow and reported that the dimensionless height of the electroconvective vortices is strongly coupled with the imposed voltage and shear velocity as $h \sim (V^2/U_{HP})^{1/3}$, where V is the applied voltage and U_{HP} is the shear velocity.[24] Recently, Lui et al. presented results from scaling analysis and DNS of electroconvection in the absence of an externally imposed shear flow. These results support a linear scaling of both the dimensionless steady-state vortex height and overlimiting current with V.[25] Similarly, studies have also shown that gravitational effects can play an important role in the onset of convective flow especially in systems with large Rayleigh numbers, where Rayleigh−Bernard convection can lead to an unstable overlimiting current and this effect becomes more pronounced as the characteristic length of the system increases.[26,27]

Many aspects of the theoretical work on electroconvection have been corroborated by experimental studies where tracer particles are generally used to obtain flow patterns. Bellon et al. used fluorescein acid to observe the electrokinetic response in different regimes (ohmic, limiting, and overlimiting) by tracking changes in the dye intensity near a cation exchange particle and membrane.[28] Similarly, Valenca et al. experimentally confirmed the effects of membrane undulations on electroconvection that was initially discovered via numerical simulations performed by Davidson et al.[19,29] By observing the flow near a patterned ion-selective membrane, they reported that the onset of convection occurred faster near the edges, which almost doubled the ion transport compared to a flat membrane. Studies have also confirmed the vortex size and growth rate scale with V in steady electroconvection by using particle image velocimetry (PIV) analysis, which is a powerful tool to examine the flow data.[30] PIV analysis has also recently been used to quantify the suppression of electroconvection in electrolytes with high MW polymer additives where significantly lower velocities were obtained.[17,18]

In this work, we present an experimental study of the multiscale nature of chaotic electroconvection using PIV analysis which has not be explored previously.[7,30−32] We specifically investigate the effect of salt concentration and voltage on electroconvection onset and evolution, and compare our results with theoretical analysis to present some salient features of chaotic electroconvection.

EXPERIMENTAL METHODS

A visualization cell was built as depicted in Figures 2a and 2b and connected to a BK Precision power supply capable of supplying a fixed voltage across the cell. The copper used as the electrodes in the cell was procured from Alfa Aesar, and the Nafion NRE-212 membrane was purchased from Sigma-Aldrich. The electrolyte was made with copper sulfate and polystyrene tracer particles (3 μm) from Sigma-Aldrich and deionized water. To observe the effect of particle charge, the zeta potential of the tracer particles was measured using a Zetasizer and was found to be below 1 mV for electrolyte concentrations ranging from 0.1 to 0.001 M; for a 0.1 mM electrolyte, the zeta potential is −5.6 mV. We note that even at the higher zeta potential, the electrophoretic mobility is still about a factor of 7 or

https://doi.org/10.1021/acs.langmuir.1c00374
Langmuir 2021, 37, 5895−5901

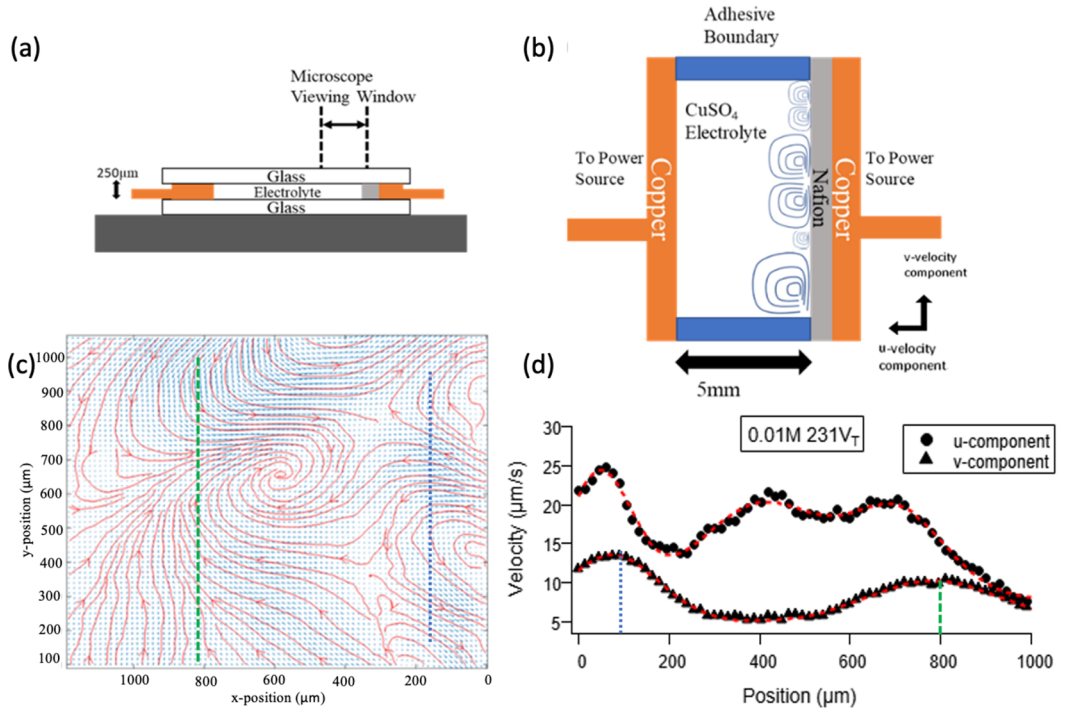

Figure 2. (a, b) Depiction of the experimental cell used for visualizing convective flow. (c) Streamline of the flow for 0.01 M $CuSO_4$ at a potential of 231 V_T. The Nafion membrane ($x = 0$) is on the right side. (d) Profile of the root-mean-squared parallel (v_{rms}) and perpendicular (u_{rms}) velocity components for the same case as (c). The location of v_{rms} peaks is shown in the corresponding streamlines profile.

more lower than the peak velocity component parallel to the electric field. For the visualization experiment, a copper electrode was placed on one side of a piece of glass, and parallel to that electrode was another copper electrode wrapped in a Nafion membrane. The edges of the glass in the interelectrode space were sealed with an adhesive strip. The electrolyte was injected into this space with a micropipette and then another glass cover plate was placed on top to seal the cell. The gap between the top and bottom glass plates was maintained fixed at 250 μm to minimize three-dimensional flow.[13] The length of both electrodes is approximately 2 cm. The spacing between the Nafion and counter electrode is 5 mm, and the microscope has a viewing window of 1.3 × 1.3 mm. The visualization setup is placed horizontally, which reduces complications from Rayleigh−Bernard type convection[26,27] because gravity is perpendicular to the electric field. An Olympus microscope paired with a CCD camera was used to record the videos. Videos were taken for approximately 5 min. The last 40 s of each video was partitioned into individual frames which were fed into the particle image velocimetry software package (PIVLab) in Matlab, which uses cross-correlation to extract velocity vectors.[33] The PIV software used multiple passes and was finally refined to a vector for every 15 × 15 μm section of the frame. Outliers were removed and then replaced via interpolation. RMS velocity variation with distance from Nafion surface was calculated by averaging in both the y coordinate and time, using the formula:

$$\langle u \rangle = \left(\frac{1}{y_1 - y_0} \frac{1}{t_1 - t_0} \int_{y_0}^{y_1} \int_{t_0}^{t_1} u^2 \, dt \, dy \right)^{1/2}$$

RESULTS AND DISCUSSION

We recorded convective flow patterns for different concentrations of copper sulfate electrolytes (0.1 M to 0.1 mM) in a wide range of dimensionless voltages ($40 \leq \hat{V} \leq 320$) and analyzed them using the particle image velocimetry package[33] to determine the root-mean-squared components of the velocity distribution in the direction normal to (u), as well as parallel to (v), the surface. The main results from these studies are summarized in Figure 1. Gross features of an electroconvective flow in a dilute aqueous copper sulfate near a cation-selective, Nafion interface are reported using vector maps (Figure 1a, c) and profiles of the root-mean-squared component of the velocity (v) (Figure 1b, d). The results capture three salient features of electroconvection. First, the RMS velocity distribution exhibits an initial maximum at a distance several tens of micrometers from the interface, i.e., substantially larger than the space charge thickness, ϵ. The size of the maximum is a strongly increasing function $\hat{V}$, increasing nearly 10-fold for a 4-fold increase in $\hat{V}$. Second, the RMS velocity decays slowly with distance, and a substantial convective flow is apparent even on length scales on the order of 1 mm from the permselective membrane. Finally, we find that the flow is structured, with a typically undulating velocity distribution, particularly at higher values of $\hat{V}$.

To further investigate the features reported above, we systematically vary the concentrations and voltages over a wide range to see the effect of changing Debye layer thickness and applied voltage on electroconvective flow. A characteristic feature of electroconvection is that it develops gradually. The first sign of incipient convective motion is the appearance of vortices that form slowly but accelerate as they extend into the bulk fluid, ultimately reaching a steady state. We find that this acceleration rate is a strong function of $\hat{V}$. For example, in a 0.001 M electrolyte at $\hat{V} \approx 80$, the vortices take about 20 s to form and an additional 60 s to become fully developed. In contrast, for $\hat{V} \approx 320$, vortices form within the first few seconds and extend into the bulk within 20 s. Figure 1a and c shows that the direction and strength of the flow varies strongly in space for $\hat{V} \approx 320$, but less so for $\hat{V} \approx 80$. At higher $\hat{V}$ the flow is more chaotic as vortices move along the membrane, collide, separate, or even combine to create structures that never appear to achieve a steady state. As the system never reaches a quasi-steady state, we present our results for the last 40 s of our

https://doi.org/10.1021/acs.langmuir.1c00374
Langmuir 2021, 37, 5895−5901

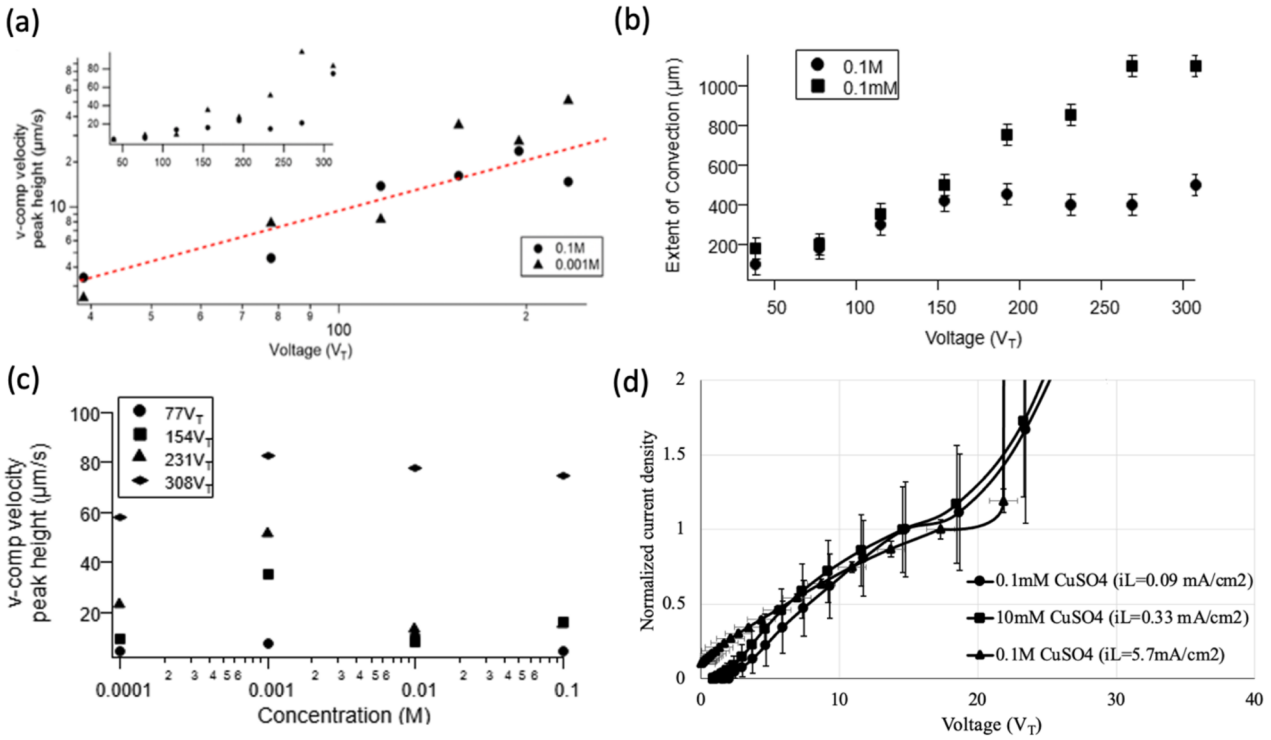

Figure 3. (a) Peak of the root-mean-squared v-component of velocity as a function of the applied potential. The dashed line depicts the scaling $V^{1.12}$. The inset shows that at higher potentials the effect of voltage is much stronger. (b) Peak of the root-mean-squared v-component of velocity as a function of the bulk electrolyte concentration for different applied potentials. (c) Extent of convection vs voltage for 0.1 mM and 0.1 M $CuSO_4$. (d) Current density−voltage (I−V) curve measured over the same range of $CuSO_4$ concentration, but at lower voltages than those used in the flow visualization experiments. The i−V curves are normalized using empirical diffusion limited current density (i_L) values for the respective electrolytes.

measurements to elucidate some key features of chaotic flow. Figure 2c reports typical particle path lines deduced from the measurements. The blue background represents the tracked vectors averaged over the last 40 s of a video taken at 231 V_T in a 0.01 M $CuSO_4$ electrolyte. Any background flow was removed by subtracting the average over each x-value. It is apparent that the velocity vector distribution has components parallel (v) and perpendicular (u) to the membrane surface. Figure 2d reports the root-mean-squared average of u and v. As with the v-component in Figure 1, at low salt concentration, u also shows evidence of structuring of the electroconvective flow. The location of the peaks in v correlates well with the size of the convective vortices observed in the videos. For example, comparing Figure 2c and 2d, the peak at 100 μm corresponds to the size of the small vortex (~150 μm) that is apparent in the vector plot. Likewise, the second peak in v at approximately 800 μm is close to the average size (~700 μm) of the second largest rolls observed (see Video S4). Comparison with streamline plots (see Video S1) reveals that the peaks in the v-component correspond to the edges of different sized vortices, with the number of associated length scales changing from primarily 2 to 3 when $\hat{V}$ increases from 78 to 315. Previous numerical simulations have reported a maximum in v, associated with the electroosmotic slip of fluid outside the ESCL and its location is associated with the ESCL thicknesses ϵ.[23] At the conditions used to obtain Figure 2d, $\epsilon \approx 8.6$ μm; the corresponding values are $\epsilon \approx 9$ μm and $\epsilon \approx 22.5$ μm for the results reported in Figures 1b and 1d. It is therefore clear that the experimentally determined first velocity maxima, v_{max}, are located well outside the calculated range for ϵ. But, we find that this first maximum in v in our case coincides with the highest root-mean-squared velocity and that its position is comparable to the length scale of the smallest vortices observed in the corresponding video. Due to linkage between vortex size and v_{max} we choose this as the velocity component of interest to study the effects of other parameters.

The effect of $\hat{V}$ on v_{max} is reported in Figure 3a. It is seen that for $\hat{V} < 230$, the relationship is approximately linear, $v_{max} \sim \hat{V}^{1.1}$. An analogous relationship has been reported in earlier galvanostatic experiments in which the size of electroconvective vortices scaled approximately linearly with current.[7,30,31] At higher potentials, the voltage has a much stronger effect on the velocity as seen in the inset in Figure 3a. Experiments and simulations support the onset of chaotic vortices at $\hat{V} > 50$ which explains the increased convective flux at the largest $\hat{V}$.[22,23,30] Figure 3b shows this effect of electrolyte concentration, 0.1 M $\leq c \leq$ 0.1 mM, on v_{max}. The Debye length δ scales with the concentration as $\delta \sim c^{-1/2}$, which at fixed $\hat{V}$ yields a scaling relationship, $\epsilon \sim c^{-1/3}$. However, from Figure 3b it can be seen that v_{max} is for all practical purposes independent of c. Figure 3d shows the effect of salt concentration on the I−V response. Over the voltage range for which stable currents can be obtained, the electrolyte salt concentration is observed to have a weak influence on the normalized I−V curve.

We further measure the extent of electroconvection in the chaotic systems which have multiple vortex sizes and peaks in the velocity profile. Figure 3c shows a comparison for the extent of convection as a function of voltage in 0.1 M and 0.1 mM $CuSO_4$ (details provided in the Supporting Information, Figure S1). At lower voltages, the extent of convection for both concentrations follows a linear scaling with potential. However,

https://doi.org/10.1021/acs.langmuir.1c00374
Langmuir 2021, 37, 5895−5901

as voltage increases the extent of convection becomes independent of voltage for higher concentration (0.1 M) and remains constant at roughly 400 μm from the surface. Meanwhile for 0.1 mM, the extent of convection keeps increasing linearly with voltage, and for voltages higher than 250 V_T, the flow occurs even beyond the experimental viewing window. Previous studies have reported a linear scaling for nonsheared electroconvection for steady vortex height, but we find this scaling valid for chaotic electroconvection too.[7,25] Figure 4 shows a comparison of the vortex size distribution for

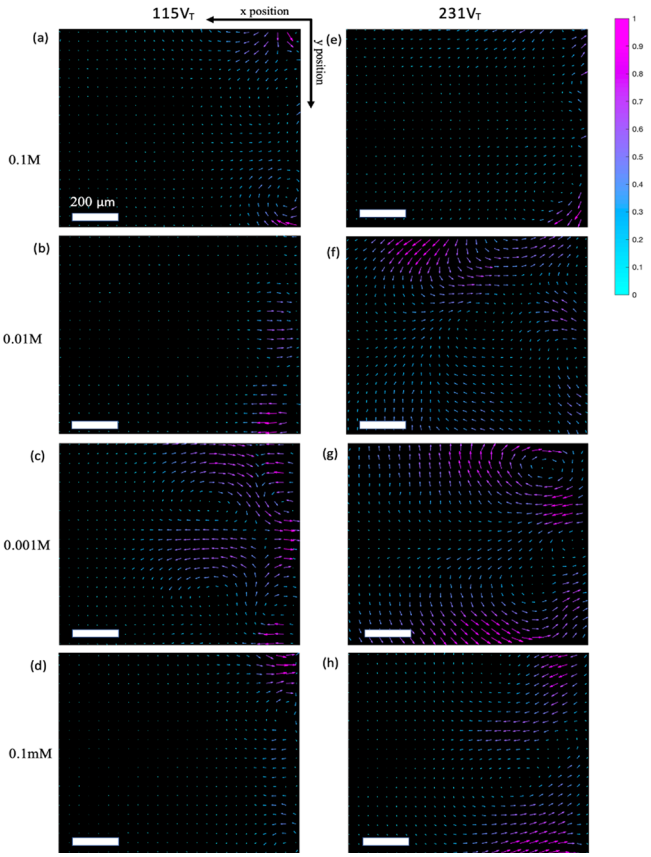

Figure 4. Vector maps of the flow for 115 V_T polarization (a–d) and 231 V_T polarization (e–h), at $CuSO_4$ concentrations of 0.1 M (a, e), 0.01 M (b, f), 0.001 M (c, g), and 0.1 mM (d, h). Each plot's vectors size and color are nondimensionalized by the maximum magnitude of that specific system. The sections with small/no vectors are regions with significantly low flow. The bounds of the axis are 0–1300 μm in both x and y.

different c and highlights the marked effect of electrolyte concentration. For example, at c = 0.1 M, vortices remain small and localized near the permselective interface (Figure 4a, e). Additionally, irrespective of $\hat{V}$, there is primarily only one velocity maximum within approximately 30 μm from the membrane surface. Looking further into the bulk there is a large reduction in convective motion. As the concentration is reduced, additional peaks in both v and u emerge. For c = 0.01 M and 0.001 M, the first velocity maximum is observed further away from the membrane surface as the smallest convective roll propagates into the bulk to distances ranging from 15 to 75 μm. These high velocity vortices appear to bring more bulk solution to the interface, which increases the effective mixing. A second peak in v is also apparent, indicating that the flow becomes multiscale. At even lower c = 0.1 mM, both the first and second maxima are observed. Notably, at $\hat{V} > 200$, a third velocity maximum begins to appear in the 0.1 mM electrolyte, showing convective flow further into the electrolyte bulk. The appearance of this third maximum coincides with the transition to a chaotic state, resulting in additional complexity of the flow structure. The large scale of the convective vortex evident in Figure 4h may also suggest the presence of flow beyond the viewing window. Thus, while we are unable to confirm/disprove the $c^{-1/3}$ relationship between the location of the first maximum in v and ϵ suggested by numerical simulations, there is a clear inverse relationship between the structure, complexity, and reach of the electroconvective flow and c. We compared the ratio of the position of these maxima to more quantitively assess the influence of ϵ on the structure of the flow. For c = 0.001 M the ratio of y_2/y_1 (ratio of second peak distance to first peak distance) is approximately 7, whereas at c = 0.01 M the ratio is roughly 22, which is consistent with an approximate scaling of $c^{1/2}$ or $\hat{\delta}^{-1}$ identified from direct numerical simulations.[34]

The multiple peaks in the velocity profile indicate the coexistence of the electroconvective vortices of different sizes and intensities. To quantify their contributions, we consider a simple analytical model where the flow is driven by a prescribed steady slip velocity of alternating signs at the bottom surface (details provided in the Supporting Information, Figure S2). The slip velocity is assumed to have simple expression $U(x) = \sin(\pi x)$ and the rms of the velocities can be easily found as $u_{rms} = \sqrt{2/1 - \pi y e^{-\pi y}/2}$ and $v_{rms} = \sqrt{\pi y e^{-\pi y}/2}$. As shown in Figure 5a, this model qualitatively agrees with the

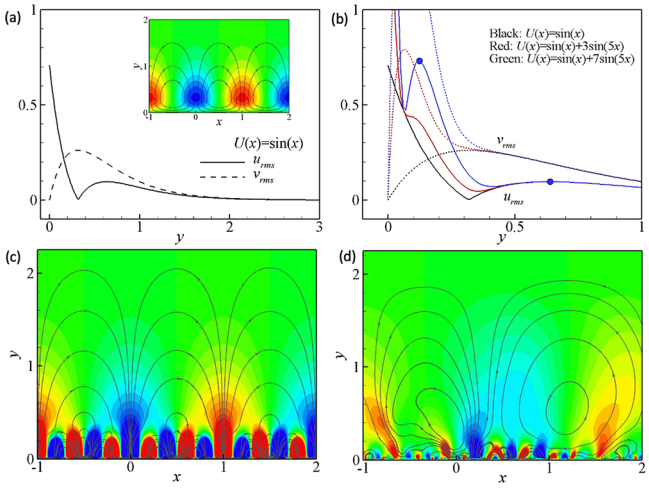

Figure 5. (a, b) Root mean square of the velocity vector field components driven by different steady slip velocities. (c) Vortex structures induced by a slip velocity $U = \sin(x) + 7\sin(5x)$. (d) A snapshot of the direct numerical simulation results of multiscale electroconvective vortices.

experiment results as shown in Figures 1 and 2. To model the multiscales in the electroconvection field, we consider a linear superimposition of two slip velocities of different length scales and intensities (Figure 5b). The corresponding flow field for $U(x) = \sin(\pi x) + 7\sin(5\pi x)$ are shown in Figure 5c. The structure of the flow assembles the direct numerical simulation results (Figure 5d) using the same method in our previous studies.[35] If the small-scale flow is strong enough, it leads to an extra peak in the normal closer to the surface. The ratios of the position and the magnitude of the two velocity peaks are

https://doi.org/10.1021/acs.langmuir.1c00374
Langmuir 2021, 37, 5895–5901

directly determined by the wavelength and magnitude of the imposed velocity, with $y_2/y_1 = 0.64/0.12 \sim 5$ and $v_1/v_2 = 0.73/0.1 \sim 7$ for the velocity $U(x) = \sin(\pi x) + 7\sin(5\pi x)$. With this observation, we can estimate the vortices in our experiment. In Figure 1b, the ratio between the first and second peaks are $y_2/y_1 \sim 300/50 \sim 6$ and $v_1/v_2 \sim 8/6$, while in Figure 1d, they are $y_2/y_1 \sim 500/100 \sim 5$ and $v_1/v_2 \sim 85/55$ and are close to the result in Figure 1b. These ratios are similar to the values obtained from the numerical simulation. This also shows that the cascade pattern of the multiscale vortices is not strongly influenced by the voltage.

CONCLUSION

In summary, we have visualized electroconvection at the interface between a cation-selective membrane and a liquid electrolyte. Through particle tracking, vector fields of the flow patterns were developed and analyzed as a function of time to study how the flow forms and grows. It is found that electroconvection can occur simultaneously on multiple length scales near permselective interfaces. The effect of increasing potential is 2-fold, with both a velocity enhancement that scales roughly linearly with applied potential and an increase in flow complexity. The electrolyte concentration has a large effect on the flow structure as quantified by the size ratio of small-to-larger vortices, which has a scaling related to the dimensionless Debye length. We also corroborate our experimental results for vortex height ratios and distances to numerical simulation results obtained from a simple model for electroconvection.

ASSOCIATED CONTENT

Supporting Information

The Supporting Information is available free of charge at https://pubs.acs.org/doi/10.1021/acs.langmuir.1c00374.

Description of the videos submitted, calculation of extent of convection (Figure S1), and theoretical analysis details (Figure S2) (PDF)
Video S1 (AVI)
Video S2 (AVI)
Video S3 (AVI)
Video S4 (AVI)

AUTHOR INFORMATION

Corresponding Author

Lynden A. Archer − *School of Chemical and Biomolecular Engineering, Cornell University, Ithaca, New York 14853, United States;* orcid.org/0000-0001-9032-2772; Email: laa25@cornell.edu

Authors

Alexander Warren − *School of Chemical and Biomolecular Engineering, Cornell University, Ithaca, New York 14853, United States*

Arpita Sharma − *School of Chemical and Biomolecular Engineering, Cornell University, Ithaca, New York 14853, United States*

Duhan Zhang − *School of Mechanical and Aerospace Engineering, Cornell University, Ithaca, New York 14853, United States;* orcid.org/0000-0001-9428-956X

Gaojin Li − *School of Chemical and Biomolecular Engineering, Cornell University, Ithaca, New York 14853, United States*

Complete contact information is available at: https://pubs.acs.org/10.1021/acs.langmuir.1c00374

Author Contributions

[§]A.W. and A.S. contributed equally to this study.

Notes

The authors declare no competing financial interest.

ACKNOWLEDGMENTS

This work was supported by the Department of Energy Basic Energy Sciences Program through award no. DE-SC0016082.

REFERENCES

(1) Block, M.; Kitchener, J. A. Polarization Phenomena in Commercial Ion-Exchange Membranes. *J. Electrochem. Soc.* **1966**, *113* (9), 947.

(2) Seno, M.; Yamabe, T. Anomalous Conduction across Ion-exchange Membranes. *Bull. Chem. Soc. Jpn.* **1963**, *36* (7), 877−878.

(3) Fang, Y.; Li, Q.; Green, M. E. Noise spectra of sodium and hydrogen ion transport at a cation membrane-solution interface. *J. Colloid Interface Sci.* **1982**, *88* (1), 214−220.

(4) Yafuso, M.; Green, M. E. Noise spectra associated with hydrochloric acid transport through some cation-exchange membranes. *J. Phys. Chem.* **1971**, *75* (5), 654−662.

(5) Frilette, V. J. Electrogravitational transport at synthetic ion exchange membrane surfaces. *J. Phys. Chem.* **1957**, *61* (2), 168−174.

(6) Lifson, S.; Gavish, B.; Reich, S. Flicker noise of ion-selective membranes and turbulent convection in the depleted layer. *Biophys. Struct. Mech.* **1978**, *4* (1), 53−65.

(7) Rubinstein, S. M.; Manukyan, G.; Staicu, A.; Rubinstein, I.; Zaltzman, B.; Lammertink, R. G. H.; Mugele, F.; Wessling, M. Direct observation of a nonequilibrium electro-osmotic instability. *Phys. Rev. Lett.* **2008**, *101* (23), 236101.

(8) Zaltzman, B.; Rubinstein, I. Electro-osmotic slip and electro-convective instability. *J. Fluid Mech.* **2007**, *579*, 173−226.

(9) Rubinstein, I.; Zaltzman, B. Electro-osmotically induced convection at a permselective membrane. *Phys. Rev. E: Stat. Phys., Plasmas, Fluids, Relat. Interdiscip. Top.* **2000**, *62* (2), 2238−2251.

(10) Maletzki, F.; Rösler, H. W.; Staude, E. Ion transfer across electrodialysis membranes in the overlimiting current range: stationary voltage current characteristics and current noise power spectra under different conditions of free convection. *J. Membr. Sci.* **1992**, *71* (1−2), 105−116.

(11) Rubinstein, I.; Zaltzman, B.; Lerman, I. Electroconvective instability in concentration polarization and nonequilibrium electro-osmotic slip. *Physical Review E - Statistical, Nonlinear, and Soft Matter Physics* **2005**, *72*, 011505.

(12) Fleury, V.; Chazalviel, J. N.; Rosso, M. Coupling of drift, diffusion, and electroconvection, in the vicinity of growing electrodeposits. *Phys. Rev. E: Stat. Phys., Plasmas, Fluids, Relat. Interdiscip. Top.* **1993**, *48* (2), 1279−1295.

(13) Huth, J. M.; Swinney, H. L.; McCormick, W. D.; Kuhn, A.; Argoul, F. Role of convection in thin-layer electrodeposition. *Phys. Rev. E: Stat. Phys., Plasmas, Fluids, Relat. Interdiscip. Top.* **1995**, *51* (4), 3444−3458.

(14) Tikekar, M. D.; Choudhury, S.; Tu, Z.; Archer, L. A. Design principles for electrolytes and interfaces for stable lithium-metal batteries. *Nature Energy* **2016**, *1* (9), 16114.

(15) Urtenov, M. K.; Uzdenova, A. M.; Kovalenko, A. V.; Nikonenko, V. V.; Pismenskaya, N. D.; Vasil'eva, V. I.; Sistat, P.; Pourcelly, G. Basic mathematical model of overlimiting transfer enhanced by electroconvection in flow-through electrodialysis membrane cells. *J. Membr. Sci.* **2013**, *447*, 190−202.

(16) Nikonenko, V. V.; Kovalenko, A. V.; Urtenov, M. K.; Pismenskaya, N. D.; Han, J.; Sistat, P.; Pourcelly, G. Desalination at overlimiting currents: State-of-the-art and perspectives. *Desalination* **2014**, *342*, 85−106.

(17) Warren, A.; Zhang, D.; Choudhury, S.; Archer, L. A. Electrokinetics in viscoelastic liquid electrolytes above the diffusion limit. *Macromolecules* **2019**, *52* (12), 4666−4672.
(18) Zhang, D.; Warren, A. J.; Li, G.; Cheng, Z.; Han, X.; Zhao, Q.; Liu, X.; Deng, Y.; Archer, L. A. Electrodeposition of Zinc in Aqueous Electrolytes Containing High Molecular Weight Polymers. *Macromolecules* **2020**, *53* (7), 2694−2701.
(19) Davidson, S. M.; Wessling, M.; Mani, A. On the Dynamical Regimes of Pattern-Accelerated Electroconvection. *Sci. Rep.* **2016**, *6*, 22505.
(20) Druzgalski, C. L.; Andersen, M. B.; Mani, A. Direct numerical simulation of electroconvective instability and hydrodynamic chaos near an ion-selective surface. *Phys. Fluids* **2013**, *25* (11), 110804.
(21) Demekhin, E. A.; Nikitin, N. V.; Shelistov, V. S. Direct numerical simulation of electrokinetic instability and transition to chaotic motion. *Phys. Fluids* **2013**, *25*, 122001.
(22) Davidson, S. M.; Andersen, M. B.; Mani, A. Chaotic induced-charge electro-osmosis. *Phys. Rev. Lett.* **2014**, *112* (12), 1−5.
(23) Druzgalski, C.; Mani, A. Statistical analysis of electroconvection near an ion-selective membrane in the highly chaotic regime. *Physical Review Fluids* **2016**, *1* (7), 073601.
(24) Kwak, R.; Pham, V. S.; Lim, K. M.; Han, J. Shear Flow of an Electrically Charged Fluid by Ion Concentration Polarization: Scaling Laws for Electroconvective Vortices. *Phys. Rev. Lett.* **2013**, *110*, 114501.
(25) Liu, W.; Zhou, Y.; Shi, P. Scaling laws of electroconvective flow with finite vortex height near permselective membranes. *Phys. Rev. E: Stat. Phys., Plasmas, Fluids, Relat. Interdiscip. Top.* **2020**, *102*, 033102.
(26) Karatay, E.; Andersen, M. B.; Wessling, M.; Mani, A. Coupling between Buoyancy Forces and Electroconvective Instability near Ion-Selective Surfaces. *Phys. Rev. Lett.* **2016**, *116* (19), 33−37.
(27) De Valença, J. C.; Kurniawan, A.; Wagterveld, R. M.; Wood, J. A.; Lammertink, R. G. H. Influence of Rayleigh-Bénard convection on electrokinetic instability in overlimiting current conditions. *Physical Review Fluids* **2017**, *2* (3), 033701.
(28) Bellon, T.; Polezhaev, P.; Vobecka, L.; Svoboda, M.; Slouka, Z. Experimental observation of phenomena developing on ion-exchange systems during current-voltage curve measurement. *J. Membr. Sci.* **2019**, *572*, 607−618.
(29) de Valença, J.; Jõgi, M.; Wagterveld, R. M.; Karatay, E.; Wood, J. A.; Lammertink, R. G. H. Confined Electroconvective Vortices at Structured Ion Exchange Membranes. *Langmuir* **2018**, *34* (7), 2455−2463.
(30) De Valença, J. C.; Wagterveld, R. M.; Lammertink, R. G. H.; Tsai, P. A. Dynamics of microvortices induced by ion concentration polarization. *Physical Review E - Statistical, Nonlinear, and Soft Matter Physics* **2015**, *92* (3), 031003.
(31) Kwak, R.; Guan, G.; Peng, W. K.; Han, J. Microscale electrodialysis: Concentration profiling and vortex visualization. *Desalination* **2013**, *308*, 138−146.
(32) Yossifon, G.; Chang, H. C. Selection of nonequilibrium overlimiting currents: Universal depletion layer formation dynamics and vortex instability. *Phys. Rev. Lett.* **2008**, *101* (25), 254501.
(33) Thielicke, W.; Stamhuis, E. J. PIVlab − Towards User-friendly, Affordable and Accurate Digital Particle Image Velocimetry in MATLAB. *Journal of Open Research Software* **2014**, *2* (1), e30.
(34) Wang, K.; Mani, A. Scale dependence of flow structures in electroconvection. In *Proceedings of the 71st Annual Meeting of the APS Division of Fluid Dynamics*; Bulletin of the American Physical Society: Atlanta, GA, 2018; Vol. *63* (13); http://meetings.aps.org/link/BAPS.2018.DFD.D07.1.
(35) Li, G.; Archer, L. A.; Koch, D. L. Electroconvection in a Viscoelastic Electrolyte. *Phys. Rev. Lett.* **2019**, *122* (12), 124501.

https://doi.org/10.1021/acs.langmuir.1c00374
Langmuir 2021, 37, 5895−5901